Coupled THM modelling of Nuclear Spent Fuel Repository in Finland

Erdem Toprak*, Sebastia Olivella† and Xavier Pintado†

* International Center for Numerical Methods in Engineering (CIMNE)
Universidad Politécnica de Cataluña
Campus Norte UPC, 08034 Barcelona, Spain
E-mail: erdem.toprak@upc.edu

† International Center for Numerical Methods in Engineering (CIMNE)
Universidad Politécnica de Cataluña
Campus Norte UPC, 08034 Barcelona, Spain
Email:sebastia.olivella@upc.edu

† B+TECH Oy, Laulukuja 4, 00420 Helsinki, Finland
Email:xavier.pintado@btech.fi

Key words: THM coupled analyses, Effect of fracture, 3D calculations

Abstract: *This paper shows results of THM analyses of a disposal scenario under investigation. The effect of rock fracture and intrinsic permeability of rock, and the presence of a gap have been analyzed. Some results of 3D modelling of repository are also discussed.*

1.2D SENSITIVITY ANALYSES

Three cases have been defined which are based on AMEC´s groundwater flow calculations. Figure 1 shows hydraulic boundary conditions of three cases. The outer boundary conditions are same for all three cases. However, there is a fracture in the wet deposition hole which induces a preferential flow and accelerates clay barrier hydration.

Normal deposition hole — Wet deposition hole — Dry deposition hole

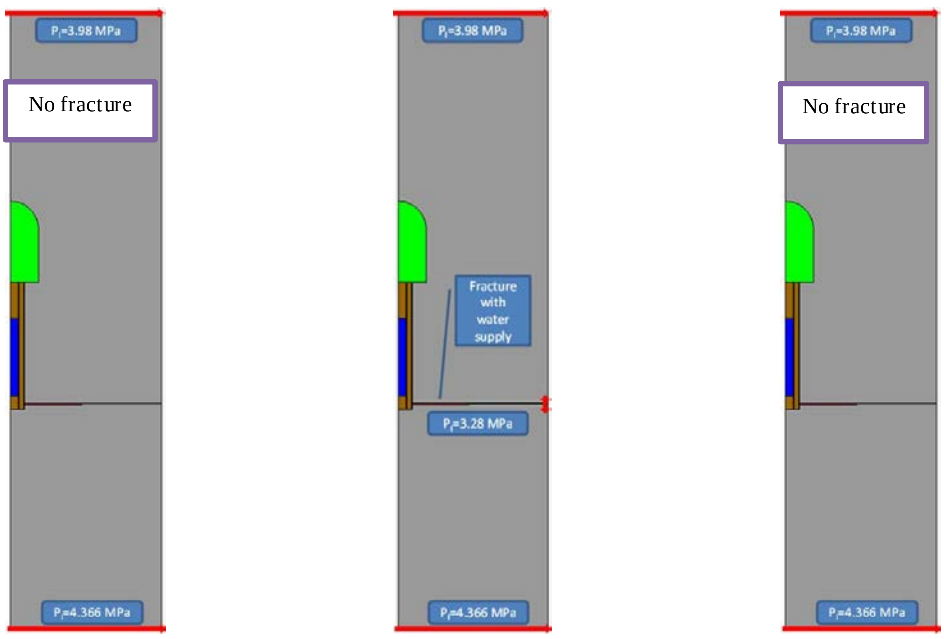

Figure 1 Properties and boundary conditions for the fracture in three cases

These three cases can be summarized as:

- Normal Deposition Hole case: The intrinsic permeability of rock is 1.52×10^{-19} m^2 (1.52×10^{-12} m/s)
- Wet Deposition Hole case: The intrinsic permeability of rock is 1.52×10^{-19} m^2 (1.52×10^{-12} m/s) and a predefined fracture that has a transmissivity of 1.2×10^{-9} m^2/s.
- Dry Deposition Hole case: The intrinsic permeability of rock is 3.53×10^{-20} m^2 (3.53×10^{-13} m/s)

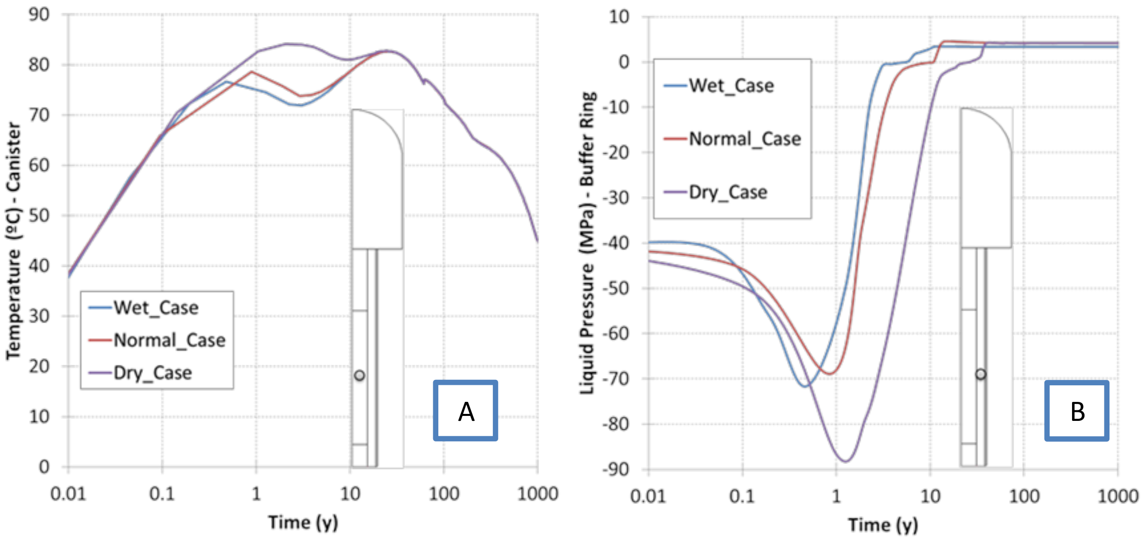

Figure 2. Evolution of temperature (A) and liquid pressure (B) in 2D calculations

Figure 2-A shows temperature evolution in the canister. The maximum temperature is not significantly influenced by permeability in general. However, the evolution at early times is different due to the effect of the gap (the gap under dry conditions produces thermal isolation). When the rock permeability is very low (Dry_Case) the gap closure is delayed and the temperature increases due to the lower thermal conductivity of the open/dry gap.

Figure 2-B shows evolution of liquid pressure for the three cases on the bentonite ring adjacent to canister. In the case of wet deposition hole, as permeability of rock is relatively higher than in the other cases (due to the presence of the fracture) saturation of materials takes place faster. Desaturation of the bentonite ring is much stronger in the Dry_Case. The effect of fracture is more obvious when the analyzed zone is close to fracture. Although the rock has the same intrinsic permeability in wet and normal cases; bentonite rings and blocks reach full saturation faster in wet case. It is a clear effect of the presence of the predefined fracture which induces an acceleration of the hydration. The time required to reach full saturation for the central zone of backfill is almost the same in wet and normal cases. The reason is that the central zone of the backfill is far away from the fracture and the time required to full saturation of backfill is mainly controlled by the intrinsic permeability of rock which is the same in normal and wet cases

The saturated density in the buffer shall be ρsat < 2050 kg/m^3 for the protection of the canister against rock shear and also must be higher than 1950 kg/m^3 to ensure a swelling pressure of 2 MPa with margin for possible loss of material (Juvankoski et al., 2012).

Figure 3 shows evolution of natural density of buffer components in wet deposition tunnel. The average natural density of buffer (it corresponds to saturated density of the buffer when the system reaches to steady state conditions) has a value 1991 to 1999 kg/m^3 depending on the case.

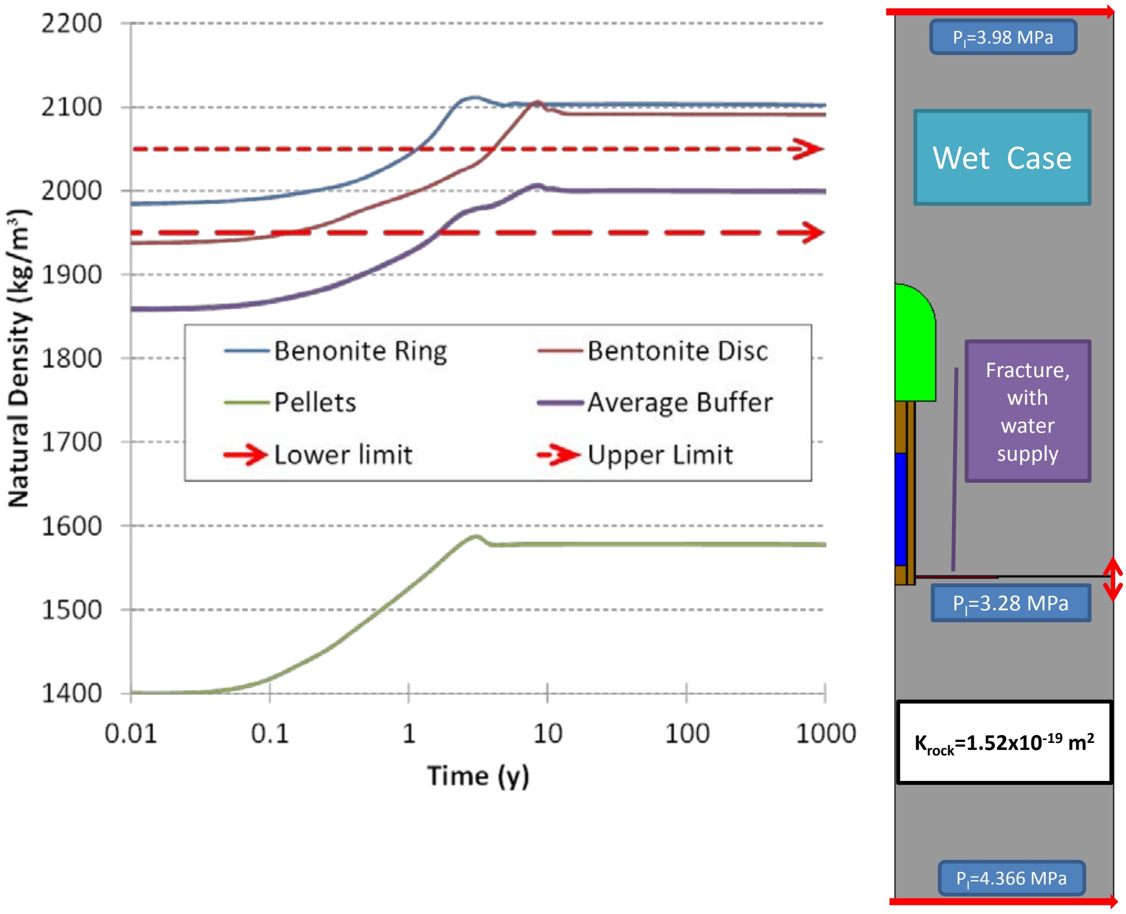

Figure 3. Average density of buffer for Wet Case

2. PRELIMINARY CALCULATIONS IN 3D

There are no pellets and air gap element in the 3D calculations. Beside this, backfill tunnel has more volume compared to the 2D calculations. Figure 4 gives a comparison between 2D (A) and 3D (B) calculations in terms of total mean stresses. As the backfill tunnel has more volume in the case of 3D calculation, the whole system needs more time to reach full saturation. Therefore, generated stresses reach the steady-state conditions in earlier times in the case of 2D calculations compared to the 3D results. However, the values achieved for the total mean stresses are quite similar and have a range of 8-12 MPa. The intrinsic permeability of rock is 1.6×10^{-20} m^2 which corresponds roughly to dry deposition hole. The other materials have been considered with permeabilities in the same range.

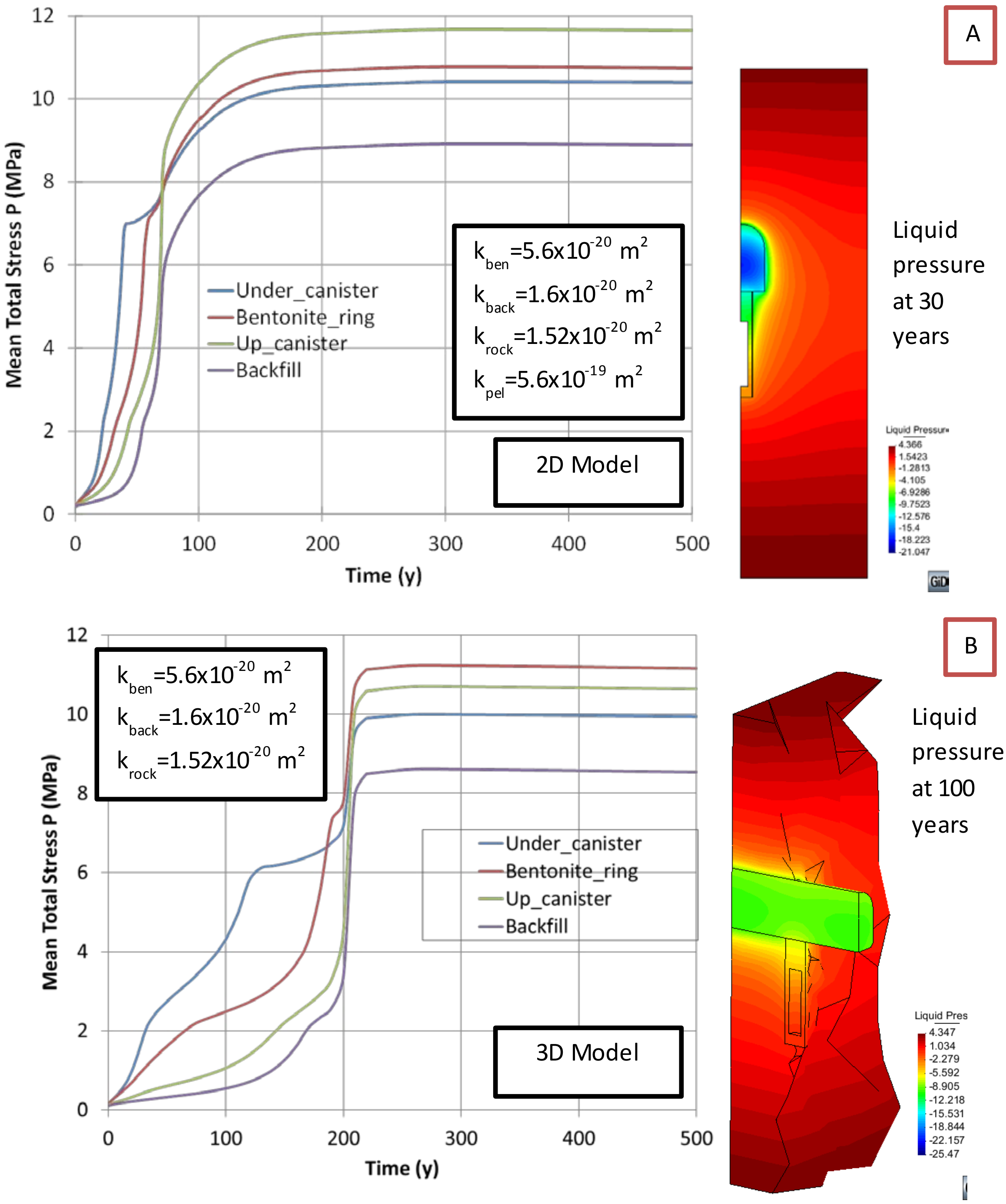

Figure 4. Evolution of mean total stresses in 2D (A) and 3D (B) modelling (left) and liquid pressure distribution at 30 years for 2D and 100 years for 3D (right).

References

Pintado, X., Rautioaho, E. (2013). Thermo-Hydraulic Modelling of Buffer and Backfill. Posiva Report 2012-48. Eurajoki. Finland.

Pintado, X., Hassan, Md, Martikainen, J. (2013). Thermo-Hydro-Mechanical Tests of Buffer Material. Posiva Report 2012-49. Eurajoki. Finland.

Toprak Erdem, Nadia Mokni, Sebastia Olivella, August 2013. POSIVA 2012-47: Thermo-Hydro-Mechanical Modelling of Buffer, Synthesis Report

INSIGHTS INTO THE RESPONSE OF A GALLERY SEALING OVER THE ENTIRE LIFE OF A DEEP REPOSITORY

D.F. Ruiz*, J. Vaunat*, A. Gens* and A. Pasteau†

* Department of Geotechnical Engineering and Geosciences. Technical University of Catalonia (UPC)
Campus Norte UPC, 08034 Barcelona, Spain.
E-mail: daniel.felipe.ruiz@upc.edu
† Agence nationale pour la gestion des déchets radioactifs (ANDRA), France

Key words: Sealing, short and long term, bentonite, concrete plug and Callovo-Oxfordian (COx)

Abstract. *A numerical modelling of the short and long term hydro-mechanical response of typical sealing systems placed in the main galleries of the future ANDRA deep nuclear waste repository is presented in this paper. The computation of model with the more fundamental characteristics of the problem (Base Case) and the contact effects that represent realistic geometrical aspects (joints, gaps, etc.) were done. The influence of more sophisticated features like a creep of the argillaceous host rock (COx) and the double structure approach for the bentonite core on the overall behaviour is also discussed although they are not modelled.*

1 INTRODUCTION

In France, the argillaceous formation *Callovo-Oxfordian (COx)* at the depth of ~500 m in the site of Meuse/Haute Marne (MHM) is considered as a potential host rock for high level radioactive nuclear waste repository. The construction of a repository will involve the sinking of a number of access shafts, the excavation of a network of horizontal access drifts and the drilling of additional horizontal drifts for waste emplacement. As pointed Gens (2003), prior to closure, it will be necessary to seal and backfill access tunnels and shafts so that they do not become preferential radionuclide migration pathways. The main purposes of seals and backfill are to provide: i) low permeability plugs ii) long term mechanical support for the underground openings, iii) additional locations for radionuclide sorption, and iv) some protection against human intrusion. The issues concerning seal behaviour are similar to those arising in the design of engineered barriers, with the important difference that no high temperatures are expected. Below is described the scheme of the seal structure for the main horizontal gallery and its numerical model.

2 CONCEPTUAL ANALYSIS OF THE PHYSICAL PHENOMENA

A tentative configuration of the seal system for the connecting galleries, ramps and shaft consists of a central core built with swelling bentonite placed between two support concrete plugs. The plugs are in contact with the filling of the gallery, made with recompacted crushed COx. (see Figure 1). The performance of these systems relies on the reach of low permeability values in the bentonite and surrounding rock (particularly in the Excavation Damaged Zone) and low transmissivity values along possible discontinuities (contacts and eventual gaps). These values depend, on the one side, on the transient hydro-mechanical processes that take place during excavation and bentonite hydration, and, on the other side, on seal long term hydro-mechanical evolution under the creep processes that will develop in the Callovo-Oxfordian. A brief description of the main steps of the seal system is done.

- Effect of excavation: excavation creates the EDZ around the openings. The main factors controlling the characteristics of the EDZ are the orientation of the gallery, the geometry of the section, the rate of excavation, the method of excavation, the time left before lining placement, the time of exposure to the relative humidity prevailing in the URL and the stress state at the

moment of excavation. The EDZ will be thus represented by ad-hoc properties determined from information obtained in several excavations in the MHM URL.
- Effect of seal installation: The installation conditions (dry density and compaction water content of the sealing material, presence of gaps and mode of eventual filling) and the transient hydro-mechanical processes determine the final dry density and stress state in the seal, the gaps and the near-field, which in turn determine the permeability of the whole system. Different scenarii such permeability reduction of the seal due to invasion of macro-voids (swelling core), the stability of the concrete plugs under the pressure developed by the seal and the role played by the lining in the load transfer from the host rock to the concrete plug are analyzed in this phase.
- Analysis of long-term effects: After water pressure equilibration between the seal and the host rock, long term creep deformation of the host rock will compress the seal system. Depending on the magnitude of compression, seal concrete elements can suffer damage, which would increase their permeability.
The modeling approach is based on the definition of different numerical models organized in a hierarchical manner.

3 FEATURE OF THE ANALYSIS

A fully coupled hydro-mechanical formulation is considered. The stress equilibrium (Eq. (1)) and water mass continuity (Eq. (2)) are solved simultaneously. For the particular case of the Base Case, vapour flow and air flow are not taken into account. As a consequence, no diffusive fluxes exist.

$$\nabla \cdot \sigma + b = 0 \quad (1) \qquad \frac{\partial (nSr)}{\partial t} + \nabla \cdot (j^{w}_{ml}) = 0 \quad (2)$$

where Sr is the degree of saturation, n the porosity and j^{w}_{ml} is related to Darcy flux. Finally the balance equations are completed by the constitutive equations.
The problem is composed by six entities: intact host rock, excavation damaged zone (EDZ), lining, concrete plugs, swelling plug and gallery filled. Some of them share materials than can be modelled by the same mechanical law (Figure 1):
- Concrete in the support plugs and the lining is modelled by linear elasticity as a first approximation.
- Host Formation (COx) and EDZ are modelled by an lastoplastic stress-strain relationship based on linear elasticity and Mohr-Coulomb yield criterion
- The response of the bentonite in the swelling plug and the disaggregated COx in the gallery is computed by the modified version of the Barcelona Basic Model (BBM) with a dependency of the elastic parameters on the mean stress and suction. This model allows obtaining a gradual increment of swelling pressure in the hydration process.
- Concerning hydraulic phenomena, the retention curve, the variation of the intrinsic permeability *Ki* with porosity n and the variation of the relative hydraulic conductivity K_r^l with degree of saturation Sr are required.
A detailed description of the above models and the all parameters is found in the reports generated by the UPC (2014).

4 BASE CASE MODELLING

The *Base Case* considers a simple bi-dimensional and axisymmetric geometry around the axis of the gallery. The whole problem has a width of 60 m and a length of 100.5 m. The outside diameter of the gallery is 8.72 m and the lining is composed of a 0.71 m thick support. Finally the sealing system includes 40.5 m long swelling core (made of bentonite), the concrete plugs are 5 m long and a fill of disaggregated and recompacted COx (considered as a non-expansive material). The total width of 3 m has been selected on the basis of data provided by ANDRA on the extension of the EDZ around galleries. The mesh has 21744 quadrilateral elements and 22003 nodes (see Figure 1).

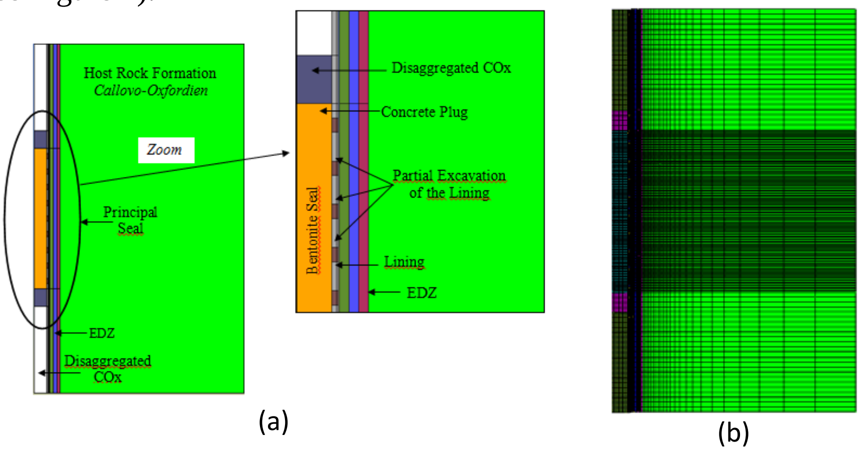

Figure 1: a) Geometry and materials includes in the basic 2D-axisymmetric modeling; b) Mesh

The stages of the modelling includes the excavation of the gallery, the installation of the lining six month later, 100 years that correspond to the work time of the repository, the sealing system installation and finally the hydration process generated by the host rock until that the initial water pressure (4.85 MPa) is recovered. In order to simulate the ventilation process during the operating time, the suction is imposed at the gallery wall (95 MPa) generated by the relative humidity (50% approximately). The anisotropic initial stress state of the COx was taken into account and the major horizontal stress is parallel to the gallery axis.

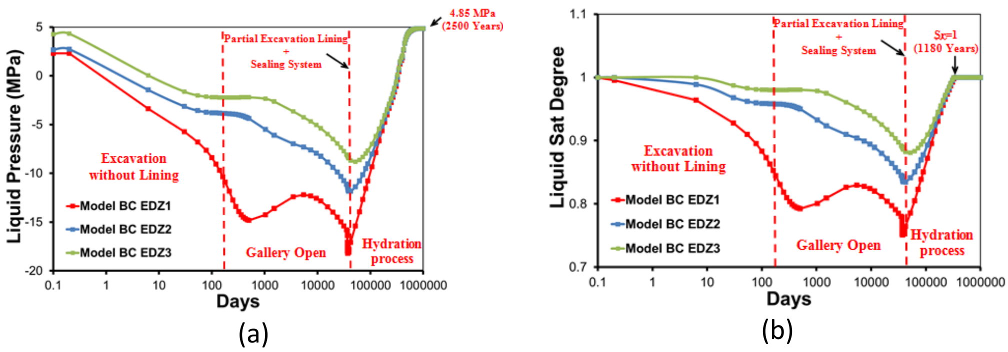

Figure 2: a) Time evolution of the liquid pressure at EDZ ; b) Time evolution the liquid saturation degree at EDZ

As a first result, the total saturation is reached at 1200 years and the initial water pressure (4.85 MPa) is recovered at 2500 years. The swelling pressure generated by the bentonite core is close to 7 MPa (Figure 2a and Figure 2b).

5 CONTACT EFFECTS MODELLING

Stress concentration appears close to at the contact between the concrete support plugs and the lining. This effect is due to the fact that the contact is considered sticken. According to the hierarchical modelling the contact effects are modelled with the joint elements implemented in Code-Bright (Zandarin 2010). The new model was computed with joint elements (Figure 4 – joints: red lines). The mechanical (elastoplastic model) and hydraulic constitutive law of the joint elements depend on the aperture (UPC 2010). The longitudinal displacement (0.20 meters) and a high value of the radial stress guarantee the stability of the sealing system. It appears indeed that, due to concrete support plug displacement, longitudinal effective stress in the swelling core decreases in a zone of 10 m close to the concrete plug, but that the swelling pressure is maintained in the center part of the core.

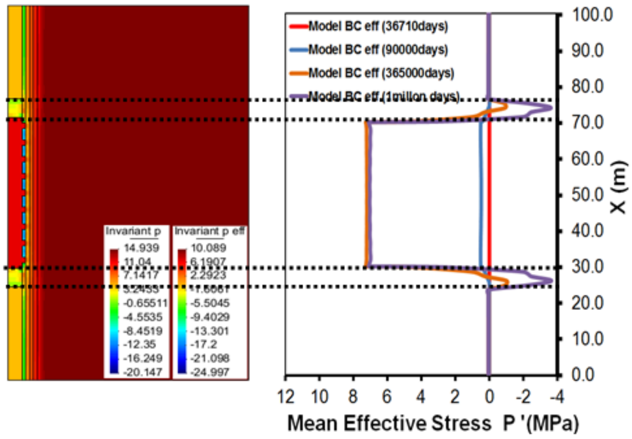

Figure 3. Swelling Pressure evolution along the sealing system axis

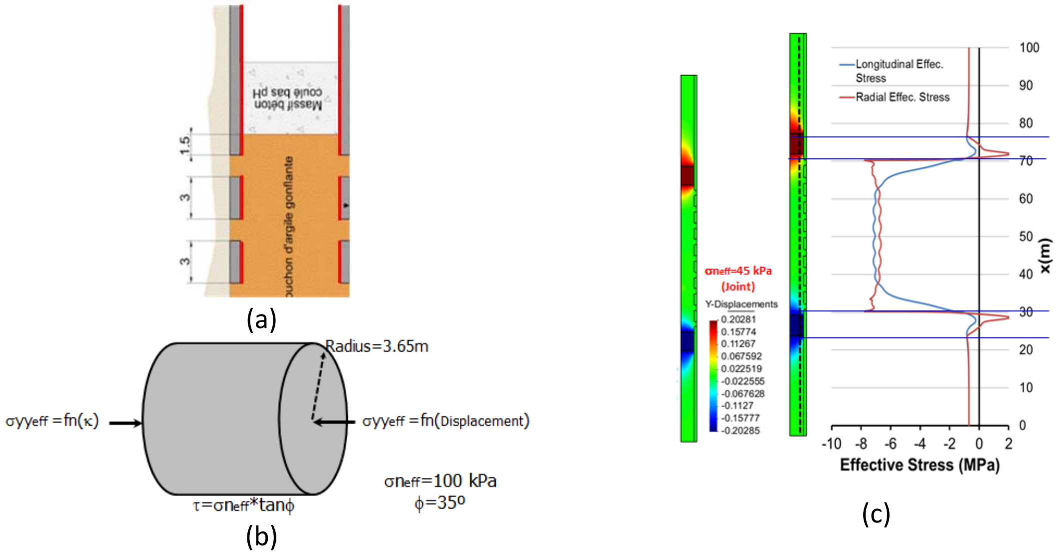

Figure 4: a) Location of joint elements; b) Forces at the concrete plug; b) Longitudinal and radial effective stresses along the sealing system

6 CONCLUSIONS AND FUTURE TASK

The double structure approach for the bentonite core is needed in order to include effects like collapse, microstructural evolution and permeability changes into hydration process.The stress state in the host rock at the end of the transient hydraulic regime is different from the initial one. This stress state may however be subjected to further variation as a result of host rock creep. This effect will be studied in forthcoming computations.

REFERENCES

- Alonso, E.E. Gens, A. Josa, A. (1990). A constitutive model for partially saturated soils. Géotechnique 40, No. 3. 405-430
- Gens, A. (2003). “The role of geotechnical engineering for nuclear utilisation”. (Special Lecture). Proc. 13th Eur. Conf. Soil Mech. Geotech. Engng, Prague 3, 25–67.
- Universitat Politècnica de Catalunya UPC. (2014). 1st and 2nd REPORT. Coupled hydromechanical simulation of the sealing system for the ANDRA deep nuclear waste repository. Project *“SCELLEMENTS”*
- Zandarin, M.T. (2010). “Thermo-Hydro-Mechanical analysis of joints - A theoretical and experimental study”. PhD Thesis. Universitat Politécnica de Catalunya (UPC).

ASSESSMENT OF FRACTURE PROPAGATION INTO THE CAPROCK DUE TO COLD CO_2 INJECTION IN DEEP SALINE FORMATIONS

Victor Vilarrasa[1] and Lyesse Laloui[1]

[1]Soil Mechanics Laboratory, Ecole Polytechnique Fédérale de Lausanne, EPFL, Switzerland
e-mail: victor.vilarrasariano@epfl.ch

Keywords: cold CO_2, thermo-hydro-mechanical couplings, induced seismicity, fracture propagation, CO_2 leakage, caprock integrity

Abstract. *Geologic carbon storage is a promising option to significantly reduce the huge amount of carbon dioxide (CO_2) that we are emitting to the atmosphere. CO_2 will generally reach the storage formation at a lower temperature than that corresponding to the geothermal gradient, especially at high flow rates. This temperature contrast induces an effective stress reduction that adds to that induced by overpressure and could compromise rock stability and induce microseismicity. Thermally induced fracture instability that may occur within the reservoir might propagate into the caprock, which could lead to CO_2 leakage. We simulate cold CO_2 injection in deep saline formations in a normal faulting stress regime. We find that the only region that yields is that of the reservoir affected by cooling, but fracture instability does not propagate into the caprock in the normal faulting stress regime simulated in this study. Thus, the caprock sealing capacity is not compromised by cold CO_2 injection and CO_2 leakage is unlikely to occur due to thermal effects.*

1. INTRODUCTION

Geologic carbon storage (GCS) is a promising option to significantly reduce the huge amount of carbon dioxide (CO_2) that we are emitting to the atmosphere [1]. GCS consists in injecting CO_2 in deep geological formations, such as depleted oil and gas fields, unminable coal seams and deep saline aquifers. Sedimentary formations are very suitable to store CO_2 because they are, in general, not critically stressed and therefore, large earthquakes that could reactivate faults are unlikely to be induced [2]. Suitable storage formations are such that their pressure (p) and temperature (T) conditions ensure that CO_2 will remain in supercritical conditions, i.e., p>7.382 MPa and T>31.04 °C [3]. This usually occurs at depths greater than 800 m. Supercritical CO_2 has a liquid-like density and a gas-like viscosity. CO_2 viscosity is around one order of magnitude lower than that of water, enabling CO_2 to flow easily within the storage formation. Storage efficiency is achieved due to the relatively high density of supercritical CO_2. However, CO_2 density is lower than that of the resident brine. Hence, CO_2 tends to float due to buoyancy (Fig. 1a). To prevent upward migration of CO_2, a low-permeability formation, known as caprock, should overly the storage formation.

CO_2 will generally reach the storage formation at a lower temperature than that corresponding to the geothermal gradient, especially at high flow rates [4]. Furthermore, if liquid (cold) CO_2 conditions are maintained along the injection well, the compression costs at the wellhead are significantly reduced [5]. Therefore, since injecting in liquid conditions is energetically efficient, many storage sites will likely inject CO_2 in liquid conditions. Cold CO_2 injection will generate a cold region around the injection well (Fig. 1b). This temperature contrast induces an effective stress reduction that adds to that induced by overpressure and could compromise rock stability [6, 7] and induce microseismicity [8, 9]. Yielding of the rock may be beneficial while it occurs within the reservoir because it opens up fractures due to dilatancy, enhancing injectivity [10]. On the other hand, thermally induced fracture instability that may occur within the reservoir might propagate into the caprock, which could lead to CO_2 leakage.

Here, we simulate cold CO_2 injection in deep saline formations in a normal faulting stress regime. Furthermore, we account for elastoplastic deformations related to fracture instability. Thus, we can evaluate the potential of thermally-induced fracture instability propagating into the caprock.

2. METHODS

We simulate cold CO_2 injection in a baserock-reservoir-caprock system in a normal faulting stress regime. Table 1 shows the thermo-hydro-mechanical properties of the rocks, which correspond to those of a permeable sandstone reservoir with homogeneous grain size [11] and a low-permeability, high capillary entry pressure shale caprock and baserock [12]. To simulate inelastic strain, we use the viscoplastic constitutive model for unsaturated soils available in CODE_BRIGHT [13, 14], which has been extended for CO_2 injection [15].

Table 1. Material properties used in the thermo-hydro-mechanical analysis of cold CO_2 injection.

Property	Reservoir	Caprock and baserock
Permeability, k (m^2)	10^{-13}	10^{-18}
Relative water permeability, k_{rw} (-)	S_w^3	S_w^6
Relative CO_2 permeability, k_{rc} (-)	S_c^3	S_c^6
Gas entry pressure, p_0 (MPa)	0.02	0.6
van Genuchten m (-)	0.8	0.5
Porosity, φ (-)	0.15	0.01
Young's modulus, E (GPa)	10.5	5.0
Poisson ratio, ν (-)	0.3	0.3
Cohesion, c (MPa)	0.01	0.01
Friction angle, ϕ' (-)	30	27.7
Thermal conductivity, λ (W/m/K)	2.4	1.5
Solid specific heat capacity, c_p (J/kg/K)	874	874
Thermal expansion coefficient, α_T (°C^{-1})	$1.0\cdot10^{-5}$	$1.0\cdot10^{-5}$

We assume initially hydrostatic conditions and that the temperature distribution follows a geothermal gradient of 33 °C/km with a surface temperature of 5 °C. The initial stress field is characterized by horizontal effective stresses equal to 0.46 the vertical effective stress. We inject 0.2 Mt/yr of CO_2 at 20 °C (liquid conditions) through a vertical well in a 20 m thick reservoir, which represents a temperature difference of 35 °C. The outer boundary has a constant pressure and temperature. The top and bottom boundaries are no flow boundaries. Displacements normal to the bottom, outer and injection well boundaries are impeded, and at the top of the caprock, a vertical lithostatic stress is applied.

3. RESULTS

Cold CO_2 injection forms a cold region that is at the same temperature than the injected fluid (Fig. 1b). This cold region advances much behind than the desaturation front (compare Figs. 1a and 1b) [16, 17]. Cooling induces contraction of the rock (Fig. 1c) and a thermal stress reduction within the reservoir in both the horizontal (Fig. 1d) and vertical (Fig. 1e) directions. These stress changes reduce the effective stresses and induce displacements. Around the injection well, the contraction due to cooling is larger than the expansion due to overpressure, which induces a downward displacement at the top of the reservoir and an upwards displacement at the bottom of the reservoir (Fig. 1f). Furthermore, the stress reduction brings the stress state towards failure conditions. Fig. 1g shows that the only region that yields is that affected by cooling. This plastic zone is related to fractures that undergo small shear slip, which may induce microseismic events [18]. Interestingly, in the normal faulting stress regime simulated in this study, this fracture instability that occurs within the reservoir does not propagate into the caprock even the strength of the caprock is lower than that of the reservoir (see Table 1). This is because the thermal stress reduction that occurs within the reservoir induces a stress redistribution that causes an increment of the horizontal stresses in the lower portion of the caprock (Fig. 1d), tightening it. Thus, the overall sealing capacity of the caprock is not compromised by cold CO_2 injection, which will be common in GCS projects. As a result, CO_2 leakage is not likely to occur across the caprock due to thermal effects.

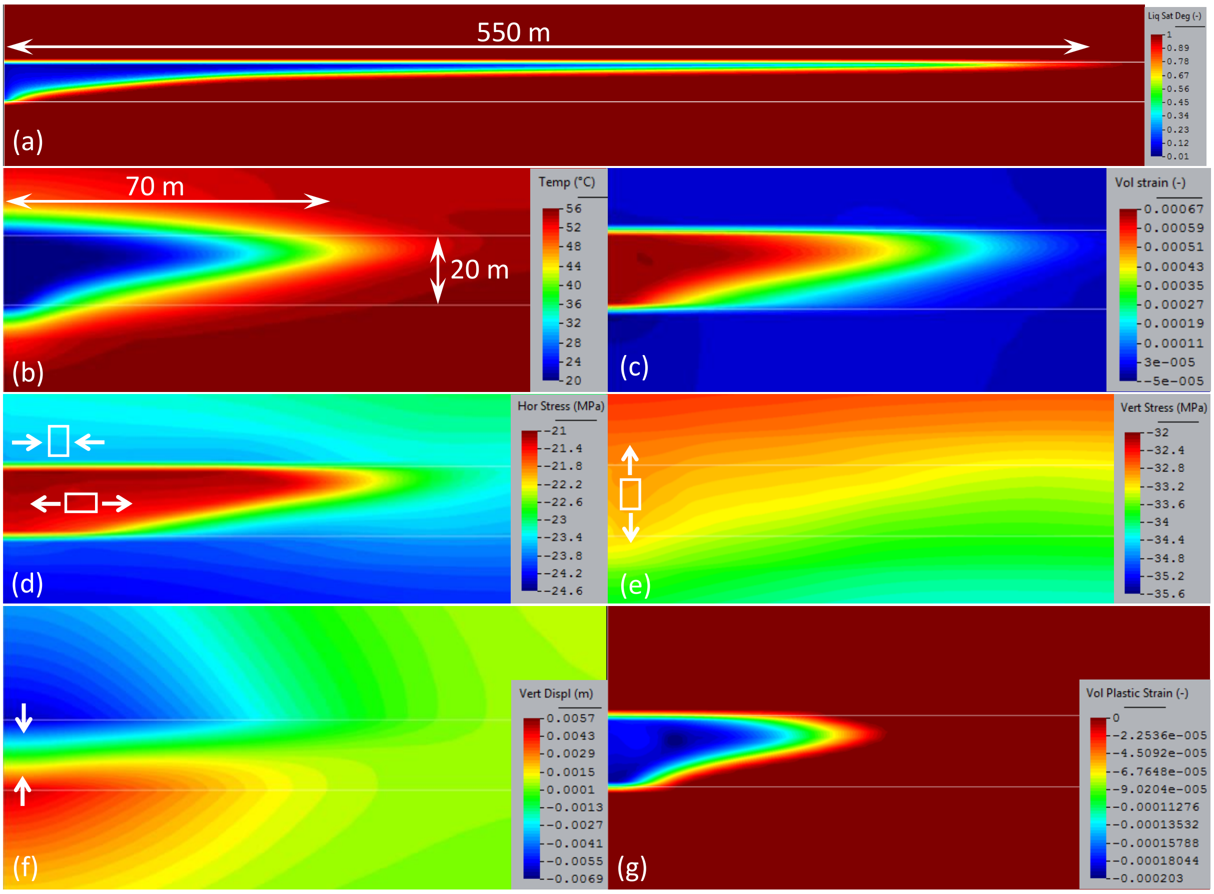

Figure 1. (a) CO_2 plume, (b) temperature distribution, (c) volumetric strain (positive sign indicates contraction), (d) horizontal total stress (negative sign indicates compression), (e) vertical total stress, (f) vertical displacement and (g) volumetric plastic strain (negative sign indicates expansion) after 2 years of cold CO_2 injection in a normal faulting stress regime.

4. CONCLUDING REMARKS

CODE_BRIGHT is a powerful numerical tool that allows studying complex coupled thermo-hydro-mechanical problems, like geologic carbon storage. In this application, we have shown that thermal effects are unlikely to negatively affect the caprock sealing integrity and that thermally-induced fractures that may occur in the storage formation are unlikely to propagate into the caprock.

ACKNOWLEDGMENTS

V.V. acknowledges support from the 'EPFL Fellows' fellowship programme co-funded by Marie Curie, FP7 Grant agreement no. 291771.

REFERENCES

[1] Hitchon, B., Gunter, W.D., Gentzis, T. and Bailey, R.T. (1999). Sedimentary basins and greenhouse gases: a serendipitous association. *Energy Conversion & Management* 40:825–843.

[2] Vilarrasa, V. and Carrera, J. (2015). Geologic carbon storage is unlikely to trigger large earthquakes and reactivate faults through which CO_2 could leak. *Proceedings of the National Academy of Sciences*, doi:10.1073/pnas.1413284112.

[3] Bachu, S. (2003). Screening and ranking of sedimentary basins for sequestration of CO_2 in geological media in response to climate change. *Environmental Geology* 44:277–289.

[4] Paterson, L., Lu, M., Connell, L.D. and Ennis-King, J. (2008). Numerical modeling of pressure and temperature profiles including phase transitions in carbon dioxide wells. *SPE Annual Technical Conference and Exhibition* Denver, 21-24 September 2008.

[5] Vilarrasa, V., Silva, O., Carrera, J. and Olivella, S. (2013). Liquid CO_2 injection for geological storage in deep saline aquifers. *International Journal of Greenhouse Gas Control* 14:84–96.

[6] Segall, P. and Fitzgerald, S.D. (1998). A note on induced stress changes in hydrocarbon and geothermal reservoirs. *Tectonophysics* 289:117-128.

[7] de Simone, S., Vilarrasa, V., Carrera, J., Alcolea, A. and Meier, P. (2013). Thermal coupling may control mechanical stability of geothermal reservoirs during cold water injection. *Journal of Physics and Chemistry of the Earth* 64:117-126.

[8] Oye, V., Aker, E., Daley, T.M., Kühn, D., Bohloli, B. and Korneev, V. (2013). Microseismic monitoring and interpretation of injection data from the In Salah CO_2 storage site (Krechba), Algeria. *Energy Procedia* 37:4191–4198.

[9] Stork, A.L., Verdon, J.P. and Kendall, J.M. (2015). The microseismic response at the In Salah Carbon Capture and Storage (CCS) site. *International Journal of Greenhouse Gas Control* 32:159-171.

[10] Rutqvist, J. and Stephansson, O. (2003). The role of hydromechanical coupling in fractured rock engineering. *Hydrogeology Journal* 11:7-40.

[11] Dana, E. and Skoczylas, F. (2002). Experimental study of two-phase flow in three sandstones. II. Capillary pressure curve measurement and relative permeability pore space capillarity models. *International Journal of Multiphase Flow* 28:1965–1981.

[12] Rutqvist, J. (2012). The geomechanics of CO_2 storage in deep sedimentary formations. *International Journal of Geotechnical and Geological Engineering* 30:525–551.

[13] Olivella, S., Carrera, J., Gens, A. and Alonso, E.E. (1994). Non-isothermal multiphase flow of brine and gas through saline media. *Transport In Porous Media* 15:271–293.

[14] Olivella, S., Gens, A., Carrera, J. and Alonso E.E. (1996). Numerical formulation for a simulator (CODE_BRIGHT) for the coupled analysis of saline media. *Engineering Computations* 13:87–112.

[15] Vilarrasa, V., Bolster, D., Olivella, S. and Carrera, J. (2010). Coupled hydromechanical modeling of CO_2 sequestration in deep saline aquifers. *International Journal of Greenhouse Gas Control* 4:910-919.

[16] Bao, J., Xu, Z. and Fang, Y. (2014). A coupled thermal-hydro-mechanical simulation for carbon dioxide sequestration. *Environmental Geotechnics* doi:10.1680/envgeo.14.00002.

[17] Vilarrasa, V., Olivella, S., Carrera, J. and Rutqvist, J. (2014). Long term impacts of cold CO_2 injection on the caprock integrity. *International Journal of Greenhouse Gas Control* 24:1-13.

[18] Vilarrasa, V., Rutqvist, J. and Rinaldi, A.P. (2015). Thermal and capillary effects on the caprock mechanical stability at In Salah, Algeria. *Greenhouse Gases: Science and Technology*, 5:1-13.

MODELLING OF A PLANNED DEMONSTRATION TEST IN ONKALO. THERMO-HYDRAULIC MODELLING INCLUDING SURFACE FRACTURE REPRESENTATIONS

Pintado X.[+] and Kristensson, O.[*]

[+]B+TECH Oy, Laulukuja 4, FI-00420 Helsinki, Finland
e-mail: xavier.pintado@btech.fi, web page: http://www.btech.fi

[*]Clay Technology AB, IDEON Science Park, S-223 70 Lund, Sweden
e-mail: osk@claytech.se, web page: http://www.claytech.se

Key words: Nuclear waste repository, "in situ" test, fracture

Abstract. *The new implementation of triangle elements between tetrahedron elements for flow and transport has been used for the simulation of the planned "in situ" test in ONKALO, Finland. The complex geometry has been implemented in GiD, taking into account the real geometry of the test and the close facility tunnels and the real position of the fractures which intersect the test area. A thermo-hydraulic analysis has been done in order to predict the evolution of the temperature and the liquid pressure during the test.*

1 INTRODUCTION

ONKALO will be used for the tests and demonstrations which really are connected to the site-specific conditions and perform the preparative experiments [1]. The key requirements for the demonstration facility in ONKALO are that the dimensions and orientation are going to be the same as planned for the deposition tunnel and the deposition hole and the bedrock conditions are going to correspond with the real disposal environment. Four tunnels have been excavated in the demo area with different lengths at the level of -420 m for the full-scale tests and demonstrations. The main purpose of the modelling is supporting the design of the instrumentation and proof that it is possible to predict the early stage of the nuclear spent fuel from the site information with the numerical tools available.

2 MODEL DESCRIPTION

2.1 Geometry and boundary conditions

The geometry and the boundary conditions are presented in Figure 1. The mesh has been created by importing the original geometry from dgn format to Solid Works, exporting from Solid Works to IGES format and importing to GiD from IGES format. The process is not automatic and some corrections should be done during the process. The modelling has been performed by using CODE_BRIGHT with its new implementation of 2-D hydraulic fractures in 3-D volumes [2]. This implementation allows for a more efficient representation of fracture networks in 3-D. The previous 3-D groundwater flow modelling concerning the demo tunnel area was performed by representing one fracture as a volume [3]. This technique, however, is not numerically efficient and only allows accounting for a limited number of fractures. The new fracture implementation, on the other hand, allows for representing the governing fractures in the mapped fracture network in ONKALO (Figure 2).

The detailed geometry and discretization of the constituents is presented in Figure 3. One of the fractures, the 002, intersected the deposition hole at the end of the tunnel. The total number of nodes was 136 505 and the total number of elements 693 439 (687 754 tetrahedrons and 5 685 triangles).

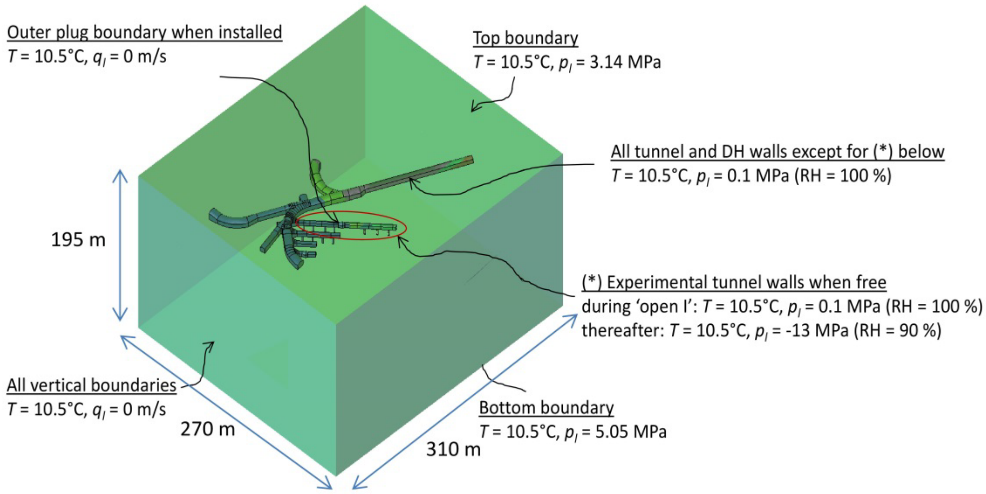

Figure 1. Geometry overview and boundary conditions. The prescribed heating power of the canisters was 410 W/m^3 (=1705 W per canister)

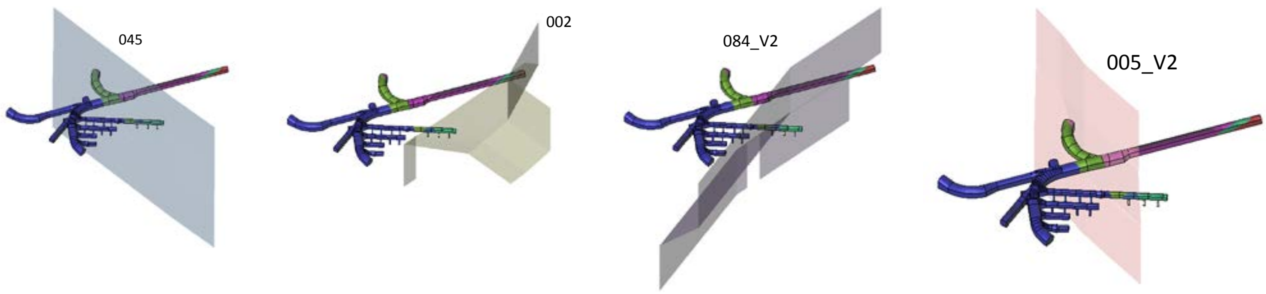

Figure 2. Fracture geometry

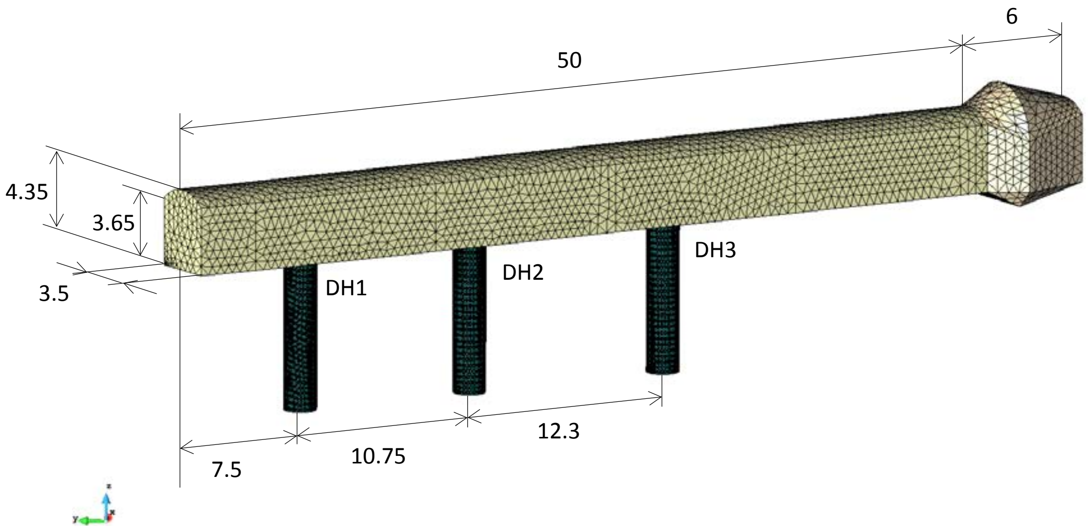

Figure 3. Geometry and discretization of tunnel backfill, plug and DHs

2.2 Material properties and initial conditions

The properties of the materials are described in Table 1. The aperture of the fracture is assumed to be 0.001 m in CODE_BRIGHT.

Constituent	n [-]	p_0 [MPa]	λ [-]	k_{ii} [m^2]	λ_{dry} [W/(m·K)]	λ_{sat} [W/(m·K)]	c_s [J/(kg·K)]	ρ_{s0} [kg/m^3]
Rock	0.005	1.5	0.3	$1.52\cdot10^{-19}$	2.61	2.61	784	2749
Fracture 045	0.005	1.5	0.3	$5\cdot10^{-15}$	2.61	2.61	784	2749
Fracture 002	0.005	1.5	0.3	$1.8\cdot10^{-15}$	2.61	2.61	784	2749
Fracture 084_V2	0.005	1.5	0.3	$5\cdot10^{-14}$	2.61	2.61	784	2749
Fracture 005_V2	0.005	1.5	0.3	$1.2\cdot10^{-14}$	2.61	2.61	784	2749
Plug	0.02	1.5	0.3	$5\cdot10^{-19}$	2.61	2.61	800	2780
Tunnel backfill	0.4602	1.5	0.3	$1\cdot10^{-17}$	0.3	1.3	800	2780
DH buffer	0.438	31.25	0.5	$5.59\cdot10^{-21}$	0.3	1.3	800	2780
Canister	0.01	31.25	0.5	$1.21\cdot10^{-35}$	8020	8020	450	7847

Table 1: Material properties

Hydrostatic pressure was adopted as the initial hydraulic condition for the rock. The initial liquid pressure in the deposition hole buffer was -41 MPa and -40.2 MPa in the tunnel backfill and plug. The initial temperature in all constituents was 10.5ºC.

3 RESULTS

The tunnels were supposed to be opened during 1200 days before the installation of the constituents. The installation was considered as t=0 and the test period were 5400 days. The liquid pressure after 360 and 5400 days are in Figure 4. The temperature after 360 and 5400 days are in Figure 5.

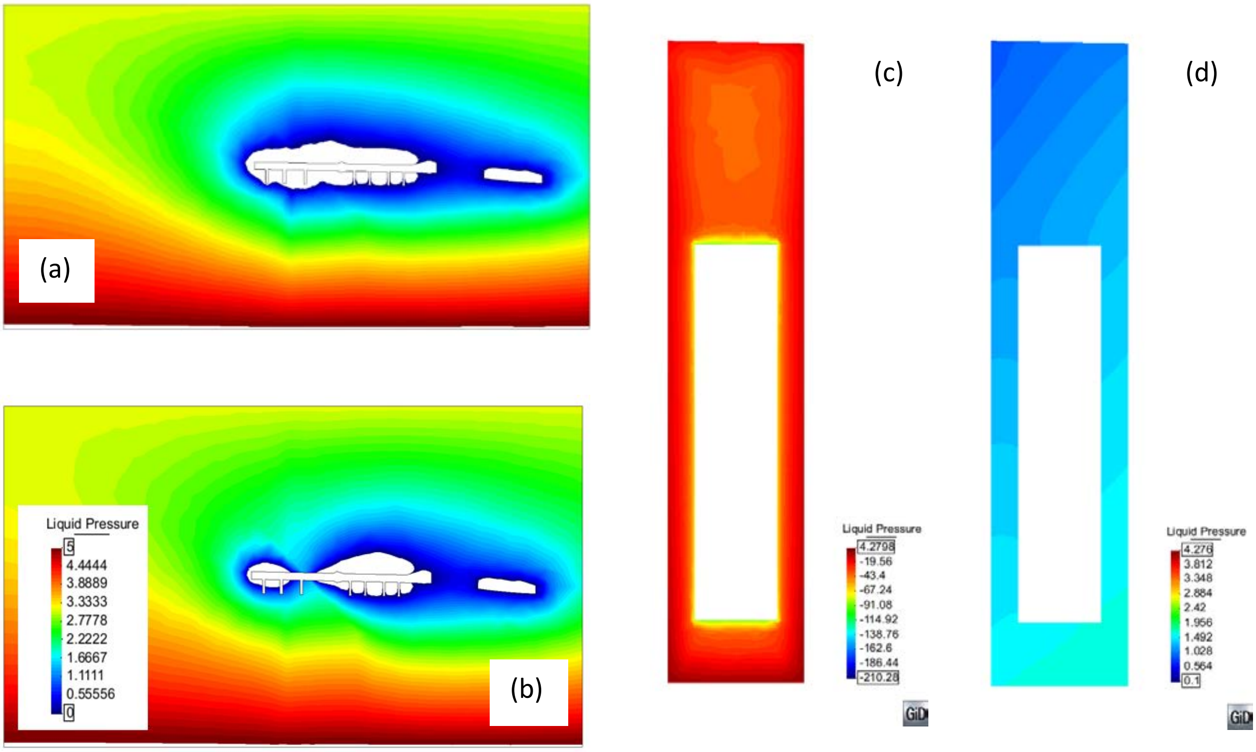

Figure 4. Liquid pressure in rock after 360 days (a). Liquid pressure in rock after 5400 days (b). Liquid pressure in deposition hole after 360 days (c). Liquid pressure in deposition hole after 5400 days (d)

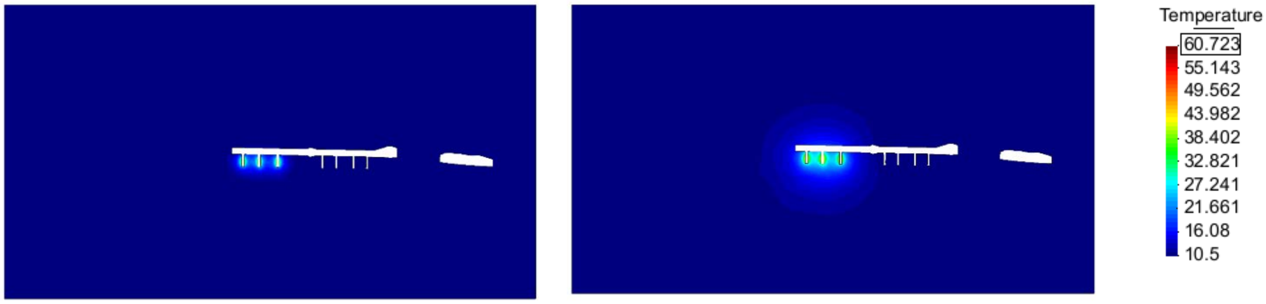

Figure 5. Temperature after 360 days (left) and 5400 days (right)

4 CONCLUSIONS

- The geometries generated with CADs can be imported to GiD but some adjustments have to be done.
- It is not possible to create surfaces inside volumes with GiD and mesh them together with the volumes. The mesh generator creates 2-D elements in the surface and 3-D elements in volume without any connection between them. The surfaces must limit the volumes, so they must be faces of volumes of rock. In this case, the number of volumes grows when some fractures have to be represented.
- Once the volumes and surfaces have been defined, the mesh generation does not have any problem because GiD is able to generate meshes in complex geometries.
- The thermo-hydraulic problem including the new surface representation of fractures can efficiently be solved using CODE_BRIGHT. The CPU time for solving the problem presented is about 26 hours on a machine with Intel Core i7, 2.93 GHz.

REFERENCES

[1] Anttila, P., Arenius, M., Haapala, K., Hansen, J., Hellä, P., Jalonen, T., Lahdenperä, J., Lyytinen, T., Mellanen, S., Vuorio, P., Äikäs, T. (2009). Testing and Demonstrations in ONKALO – Aims and Needs. Posiva report 2009-24. Posiva Oy, Eurajoki, Finland.

[2] Olivella, S. (2014). Implementation in CODE_BRIGHT of triangle elements between tetrahedron elements for flow and transport. 6th Workshop of CODE_BRIGHT users. Barcelona. Spain.

[3] Pintado, X., Rautioaho, E. (2015). Preliminary TH modelling of two deposition holes in Demonstration tunnel 2. Posiva Working report. Eurajoki, Finland.

FORMULATION OF STRAIN-GRADIENT MODEL FOR MULTIPHASE FLOW IN DEFORMABLE POROUS MEDIA

Sciarra G.[*] & Vaunat J.[†]

[*]Department of Chemical Engineering Materials & Environment
University of Rome La Sapienza
via Eudossiana, 18, 00184 Rome, Italy
e-mail: giulio.sciarra@uniroma1.it

[†]Department of Geotechnical Engineering and Geosciences
Technical University of Catalonia (UPC)
Campus Norte UPC, 08034 Barcelona, Spain
e-mail: jean.vaunat@epc.edu

Key words: Phase field, Poromechanics, Strain gradient, Capillarity

Abstract. *A poromechanical model of partially saturated porous media is proposed based on a phase field approach, the phase field being the saturation. While the standard retention curve is expected still to provide the intrinsic retention properties of the porous skeleton, depending on the porous texture, an enhanced description of the surface tension between the wetting and the non-wetting fluid, occupying the pore space, is stated considering a regularization of the phase field model based on an additional contribution to the overall free energy depending on the saturation gradient. An enhanced constitutive relation for the capillary pressure is established together with a generalization of Darcy's law.*

1 INTRODUCTION

The constitutive characterization of partially saturated porous media became of interest at the middle of the last century when scientific research started to face fundamental problems in geotechnics and petroleum engineering, concerning the response of partially imbibed soils, during drainage-imbibition cycles, or modeling the behavior of sedimentary reservoir rocks, when a multi-phase fluid flows through the porous space. Starting from the analysis of basic static problems, it became clear that the balance between capillary and driving forces, in particular gravitational forces, would have been the central subject of modeling efforts. This pushed the research in the direction of finding out a relation between the curvature of the wetting/non-wetting fluid interface and the average content of the wetting fluid, say the retention curve for the macro-scale capillary pressure. This has been for long time the only relation used for describing the hydraulic flow through partially saturated porous media, being also the pivot of the hydro-mechanical coupling with the constitutive law of the porous skeleton, see e.g. Alonso[i]. At the same time the pioneering papers by Cahn & Hilliard[ii] established the basic framework within which modeling of multi-phase fluid flow is formulated in terms of space and time evolution of a phase field which can vary continuously over thin interfacial layers. Surface tension is recovered, in this context, considering the integral, through the thickness of the layer, of the gradient of the phase field. This approach progressively attracted more and more interest, in particular within fluid mechanics, because of its advantages for numerical calculations; however limited contributions attempted at incorporating these ideas into modeling of unsaturated porous media[iii].

In this paper a novel general approach is developed which aims at merging phase field modeling of multi-phase fluid flow with unsaturated strain gradient poromechanics. While the standard retention curve is expected still to provide the intrinsic retention properties of the porous skeleton, depending on the porous texture, an enhanced description of surface tension between the wetting and the non-wetting fluid, occupying the pore space, is stated considering a regularized phase field model.

2 THERMODYNAMICS

Thermodynamics of porous media has been summarized by Coussy[iv] for two monophasic superimposed interacting continua, say the solid skeleton and the fluids saturating the porous space. In this case, the specific internal energies of the fluids are separately defined, whether they are in the liquid or in the gaseous phase; whilst the energy due to interfacial interactions between the fluids and among the solid and the fluids are incorporated into the macroscopic energy of the skeleton. Here a novel approach is adopted in order to incorporate, into the macroscopic constitutive prescription, the role of the interface between a liquid (water) and a gas (wet air), describing the mixture as a non-uniform diphasic fluid, which can reside in the liquid or in the gaseous phase. The fluid internal energy is given by:

$$\mathscr{E}_f = n\rho_f e_f(1/\rho_f, s_f) + \kappa_f(f_\rho), \qquad f_\rho = \delta_{\alpha\beta}(n\rho_f)_{,\alpha}(n\rho_f)_{,\beta} \tag{1}$$

where $\rho_f e_f$ is a double-well potential depending on the mass density, per unit volume of the mixture, ρ_f and the specific entropy s_f, n being the Eulerian porosity. The non-local energy κ_f penalizes the formation of interfaces and provides a regularization of the non-convex energy $\rho_f e_f$. The state equation of the fluid defines the fluid thermodynamic pressure $\mathcal{P}$ and the fluid chemical potential μ, in terms of the the mass density ρ_f:

$$\wp = -\partial e_f / \partial(1/\rho_f), \qquad \mu = \partial(\rho_f e_f)/\partial\rho_f, \tag{2}$$

however, because of eq.(1), these last quantities are not sufficient to characterize the complete constitutive law of the non-uniform fluid, which conversely necessitates of specifying the so-called fluid hyper-stress vector. Incompressibility of the liquid phase implies the variation of ρ_f to be univocally determined by the variation of the saturation degree S_r, $\rho_f = \rho_L S_r$, ρ_L being the intrinsic constant density of the liquid phase. Thus the liquid (gaseous) phase corresponds to $S_r = 1$ ($S_r = 0$). Assuming a Duffing potential for the volumetric energy one has:

$$\Psi_f = \rho_f e_f = C(\gamma_{nw}/R) S_r^2 (1 - S_r)^2 \tag{3}$$

where γ_{nw} is the surface tension between the non-wetting and the wetting phase and R the characteristic size of the channel through which the fluid can pass. The non-local term is typically assumed quadratic in the gradient of nS_r.

The first and the second principle of thermodynamics, together with the expression of the internal working relative to a strain gradient porous continuum[v], allow to state the constitutive prescriptions for the overall stress and hyper-stress, say S_{ij} and P_{ijk}, required to verify the overall balance of momentum $(S_{ij} - P_{ijk,k})_{,j} + b_i = 0$, as well as the generalized constitutive characterizations of the capillary pressure $\mathcal{P}_c$ and the fluid hyper-stress vector γ_k

$$S_{ij} = S'_{ij} - (\wp - S_r \wp_c)\delta_{ij} - \gamma_k (2E_{ij,k} - \delta_{ij}(nS_r)_{,k}/\phi_0 S_r), \qquad S'_{ij} = \partial\Psi_s/\partial E_{ij} \tag{4}$$

$$P_{ijk} = P'_{ijk} - \gamma_k \delta_{ij}, \qquad P'_{ijk} = \partial\Psi_s/\partial E_{ij,k} \tag{5}$$

$$\phi\wp_c = -\partial\Psi_s/\partial S_r + \gamma_k/S_r J_{,k}/J, \qquad \gamma_k/(\phi S_r) = -\partial\Psi_s/\partial(\phi S_r)_{,k} \tag{6}$$

ϕ and ϕ_0 being the Lagrangian porosity and its initial value. Eqs. (4)-(6) hold true within the assumption of small elastic strains. S'_{ij} and P'_{ijk}, are the generalized effective stresses, prescribed in terms of the partial derivatives of the skeleton free energy $\Psi_s = \Psi - \phi\Psi_f$ with respect to strain and strain gradient, Ψ being the free energy of the overall porous continuum.

Thermodynamics also implies the dissipation relative to the fluid to be positive, away from stationarity, which yields the generalized form of Darcy's law:

$$-\wp_{,k}/S_r + [\wp_c - (\gamma_l/(nS_r))_{,l}]_{,k} + b_k^f/(\phi S_r) = A_{kl} M_l/\rho_L, \tag{7}$$

where M_l is the Lagrangian filtration vector and A_{kl} the inverse of permeability. Introducing the capillary energy U, so that $\partial\Psi_s/\partial S_r = \phi\,\partial U/\partial S_r$, implies eq.(7) to be rephrased as follows:

$$-[\partial(\Psi_f + U)/\partial S_r - (\partial\Psi_s/\partial(\phi S_r)_{,l})_{,l}]_{,k} + b_k^f/(\phi S_r) = A_{kl} M_l/\rho_L. \tag{8}$$

The role of the capillary energy U is therefore that of modifying the double-well potential Ψ_f which prescribes the free energy of the fluid, in order to account for the wetting properties of the solid skeleton. The new free energy Ψ_f+U, which can be called effective energy of the pore-fluid, has not the same minima as Ψ_f, as these are shifted inward the interval (0,1) from below or from above, whether the solid skeleton is gas or liquid wet.

3 CHARACTERIZATION OF THE PORE-FLUID

Providing a constitutive characterization of the pore-fluid, say of the fluid within the pore network, is generally achieved, in unsaturated poromechanics, assuming a the capillary pressure $\mathcal{P}_c$, as a function of S_r. Here the liquid-gas mixture, which saturates the pore space, is regarded as a non-uniform fluid, the corresponding saturation ratio being used to characterize the state of the fluid at any current placement. No distinction is therefore made explicit between the pressure of the liquid and the pressure of the gaseous phase, as well as between the corresponding chemical potentials. Moreover no explicit algebraic relation between the saturation degree and the capillary pressure or the chemical potential of the fluid can a-priori be stated, without solving, at least at equilibrium, the following equation:

$$d(\phi S_r)/dt - \{K_{sat} k(S_r)[(\partial(\Psi_f + U)/\partial S_r - (\partial\Psi_s/\partial(\phi S_r)_{,l})_{,l})_{,k} + b_k^f/(\phi S_r)]\}_{,k} = 0 \tag{9}$$

which reads as a generalization of Richards' equation. Here the permeability of the porous medium has been assumed isotropic: $(A^{-1})_{kl} = K_{sat}\, k(S_r)\ \delta_{ij}$, K_{sat} and $k(S_r)$ being the so-called saturated and relative permeabilities of the wetting phase, respectively. At stationary conditions, eq.(9) reduces to a fourth order partial differential equation in the space variable, which is definitely similar to the one prescribing the mass density distribution of a Cahn-Hilliard fluid at equilibrium. However a fundamental additional term is here accounted for, say the derivative of U with respect to S_r, which allows for describing the confining effect on the non-uniform fluid, due to the presence of the porous skeleton.

In order to numerically implement eq.(9) within a FE code (CODE_BRIGHT), it is useful to rephrase it, in terms of two partial differential equations, as follows:

$$\begin{gathered} d(\phi S_r)/dt - \{K_{sat} k(S_r)[\mu^{eff}_{,k} + b_k^f/(\phi S_r)]\}_{,k} = 0, \\ \mu^{eff} = \partial(\Psi_f + U)/\partial S_r - (\partial\Psi_s/\partial(\phi S_r)_{,l})_{,l}. \end{gathered} \tag{10}$$

The role of Ψ_f and U in the characterization of the distribution of S_r, μ and $\mathcal{P}_c$ deserves a deeper analysis. Consider the chemical potential of the pure fluid, prescribed by eq.(2), say

$$\mu=\partial\Psi_f/\partial S_r=(\rho_L g)h_f, \quad h_f=2C(\gamma_{nw}/(\rho_L g R))S_r(1-3S_r+2S_r^2), \tag{11}$$

and the derivative of the capillary energy, given by the van Genuchten curve relative to a sand

$$\partial U/\partial S_r=-(\rho_L g)h_U, \quad h_U=(1/\alpha)\{[(S_r-S_r^{res})/(1-S_r^{res})]^{-1/m}-1\}^{1/n}. \tag{12}$$

depicted in figure 1(a) (gray dotted and gray dashed lines). The profile of the negative effective chemical potential of the pore-fluid $\mu+\partial U/\partial S_r$ with respect to S_r is also drawn (solid line). Both the chemical potential and the derivative of the capillary energy are expressed in head units adopting the classical Leverett scaling, which prescribes the characteristic length R in terms of the intrinsic permeability of the soil: $R=\sqrt{\kappa/\phi_0}$. The negative effective chemical potential exhibits a non-monotonic behavior and two additional zeros (the spots) with respect to the one at S_r=1, which can always be found. This feature corresponds to the fact that the energy Ψ_f+U maintains the double-well shape typical of Ψ_f, see figure 1(b). However the two minima of Ψ_f+U are no more isopotential and the one associated to smallest value of S_r is shifted inwards the interval (0,1).

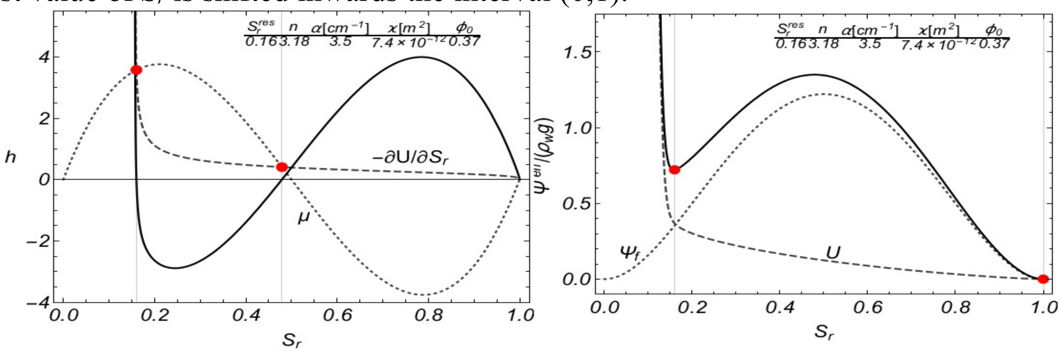

Figure 1: In panel (a), heads of the chemical potential μ of the pure fluid (dotted gray line), the derivative of the capillary energy (dashed gray line) and the effective chemical potential $\mu+\partial U/\partial S_r$ (solid black line); in panel (b) the corresponding energies. The parameters which characterize the retention curve are those of a sand.

4 CONCLUSIONS

- Gradient theory of poromechanics together with a phase field approach have been used to model partial saturation.
- An enhanced version of Richards' equation has been deduced, which depends on the so-called generalized chemical potential, accounting for the retention properties of the solid and the diphasic nature of the non-uniform saturating fluid.

REFERENCES

[i] Alonso E.E., A. Gens, A. Josa, 1990. Constitutive model for partially saturated soils. Géotechnique, 40 No 3, pp:405-430

[ii] Cahn J.W., J.E. Hilliard, 1958. Free energy of a nonuniform system. I. Interfacial free energy. The Journal of Chemical Physics, 28 No 2, pp: 258-267

[iii] Papatzacos P., S.M. Skjæveland, 2004. Relative permeability from thermodynamics, SPE Journal, 9 No 1, pp: 47-56

[iv] Coussy O., 2004. Poromechanics. John Wiley & Sons: New York

[v] Sciarra, G., dell'Isola F., Coussy O., 2007. Second gradient poromechanics. International Journal of Solids and Structures, 44 No 20, pp: 6607-6629.

MODELLING THE LONG-TERM DEFORMATION BEHAVIOUR OF CONCRETE BASED SEALING MATERIALS IN ROCK SALT RELATED TO THE DOPAS PROJECT

O. Czaikowski, K. Jantschik & K. Wieczorek

Gesellschaft für Anlagen und Reaktorsicherheit (GRS) gGmbH
Theodor-Heuss-Strasse 4, 38122 Braunschweig, Germany
e-mail: oliver.czaikowski@grs.de, web page: http://www.grs.de

Key words: sealing materials, rock salt, salt concrete, modelling, DOPAS

Abstract. *The work is related to the research and development on plugging and sealing for repositories in salt rock and is of fundamental importance for the salt option which represents one of the three European repository options in addition to the clay rock and the crystalline rock options. This paper presents selected experimental findings, obtained by GRS as part of the European project DOPAS, which are interpreted by physical modelling and numerical simulation using CODE_BRIGHT. Within the interpretative modelling process, 2D numerical modelling work is performed and the simulation results are compared to the experimental findings.*

1 INTRODUCTION

In the German concept for the final disposal of radioactive and hazardous waste in salt formations, cement based systems are proposed as technical barriers (shaft and drift seals). Due to the specific boundary conditions in salt host rock formations these materials (salt and sorel concretes) contain crushed salt instead of sand or gravel. The programme aims at providing experimental data needed for the theoretical analysis of the long-term sealing capacity of these sealing materials.

In order to demonstrate hydro-mechanical material stability under representative load scenarios, the long-term deformation material behaviour as well as the sealing capacity of the seal, a comprehensive laboratory testing programme is carried out.

This paper presents selected results of the work performed by GRS as part of the European project DOPAS[i] (Full scale Demonstration of Plugs and Seals) under WP 3 on "Design and technical construction feasibility of the plugs and seals" and and WP 5 on "Performance assessment of plugs and seals systems".

2 LABORATORY INVESTIGATIONS

2.1 Testing material

Salt concrete is a mass concrete that is used for the construction of dam structures or for backfilling of drifts in rock salt. Backfilling of excavations and construction of dam structures aims at preserving the integrity of the geological barrier, at stabilizing the disturbed rock zone at the contour and at limiting and decelerating inflow of brine.

Specimens for uniaxial creep tests were extracted from an in situ construction in a former salt mine. The drift sealing element was constructed at the 945 m level in January 1992. Its dimensions are 8.0 m length, 5.5 m width and 3.4 m in height. The sealing function is influenced by three factors: the salt concrete itself, the contact zone between concrete and host rock and the excavation damaged zone (EDZ).

The specimens used by GRS for the laboratory tests were extracted from boreholes B4 and B5. (Compare to Fig. 1). At this time the salt concrete had been exposed to the convergence of the rock salt for about ten years.

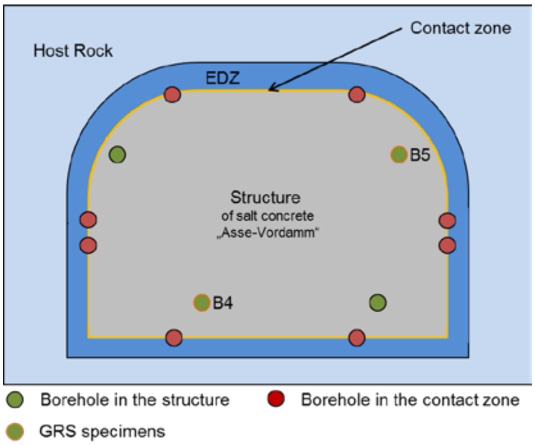

Fig. 1: Definition of the three parts of a sealing system and identification of the borehole

Fig. 2: Salt concrete sample before testing

The average porosity of the samples is about ϕ = 6 % with a grain density of 2.17 – 2.2 g/cm^3. The average residual water content is about w = 2 weight-%. Fig. 2 clearly shows the open voids (artefacts from hydration process) marked in red and filled with resin during the sample preparation procedure.

Salt concrete consists of a matrix from cement with inclusions of crushed salt. The proportion is defined in Tab. 1.

Components of salt concrete	Proportion in [kg/m^3]	Proportion in mass-%
Blast furnace cement	380	18.3
Crushed salt	1.496	72.1
NaCl-brine	198	9.5
Total	2.074	100.0

Table 1: Components of salt concrete

2.2 Long-term deformation behaviour

Within the project, two types of tests were carried out: Triaxial compression tests and uniaxial creep tests. In this paper, only the results from uniaxial creep tests were shown and compared to the calculation results using CODE_BRIGHT.

Uniaxial creep tests were performed in five rigs in an air-controlled room. One rig allows five samples to be simultaneously tested at the same load up to 500 kN at ambient temperature. Axial load was applied equally to the five samples by means of an oil balance with accuracy higher than ±0.5 %. Axial deformation of each sample was originally measured by displacement transducers (LVDT) with an accuracy of ±0.1 mm. The strain measurement was then improved by several strain gauges of higher solution of 10^{-6}. They were directly glued on the samples for both axial and radial strain measurements.

3 PHYSICAL MODELLING AND NUMERICAL SIMULATION

3.1 Physical modelling

In the framework of the presented modelling exercise the computer code CODE_BRIGHT developed by UPC is used for 2D analysis of coupled thermo-hydro-mechanical (THM) phenomena in geological media. The idea of GRS' simulations is to use classical creep models validated for rock salt and installed in CODE_BRIGHT to try to model the evolution of salt concrete with time.

Details about the basic theories with the formulated governing equations are described in the code manual[ii]. The constitutive equations establish the link between the independent variables and the dependent variables. They are assigned to the material parameters compiled in Table 2, which are published in a recent report[iii].

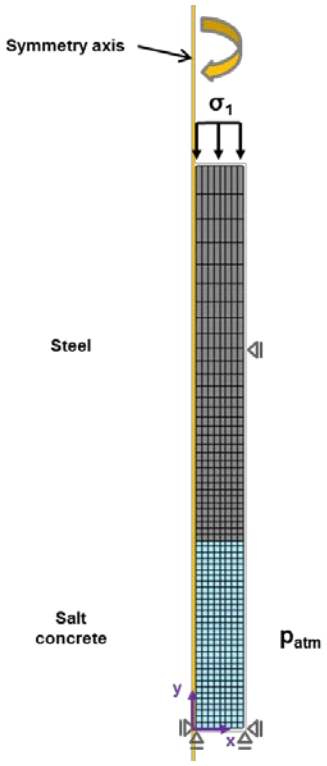

Fig. 3: Specimen for the UCc-Test

For simulation of the uniaxial creep test, a representative model was designed. The length of the salt concrete specimen is 160 mm and the length of steel piston is 320 mm, as shown in Fig. 3. Due to the symmetry of salt concrete specimen this model was generated in terms of an axial symmetric 2-D model. Consequently the width of this model is 40 mm.

Boundary conditions were generated as nodal forces at the bottom of the salt concrete specimen and as collateral ones at the steel piston. They constrain displacements in horizontal and vertical direction at the bottom of the salt concrete and horizontal displacements at the steel piston. The fixed boundary condition at the bottom does not represent the situation in the laboratory, but was necessary for numerical calculations. Axial stress was modelled as boundary stress at the top of steel piston. The axial stresses (σ_1) reached from 5 MPa to 20 MPa. An atmospheric pressure (p_{atm}) of 0.1 MPa was applied radial to the salt concrete specimen.

Initial temperature, stress and porosity were generated on the surfaces of salt concrete and steel piston. The mesh of this model was carried out with rectangular elements. The salt concrete was meshed with 256 quadratic elements using the same dimension. The feed size averages 0.5 mm in each case. The steel piston consists of 256 elements. These elements are nearly quadratic at the boundary layer to the salt concrete and become elongated in vertical direction. The reason was to get a finer discretization near the boundary layer. The number of nodes for the whole model was 585. The mesh is shown in Fig. 3. Due to the layout of the mesh, displacements at the contact zone between salt concrete specimen and steel piston are not possible.

3.2 Experimental findings compared to simulation results

The calculation results shown in Fig. 4 indicate that deformations increase with higher values of the factor a_1. The laboratory results are well covered by using a_1 from 1.8 up to 1.9.

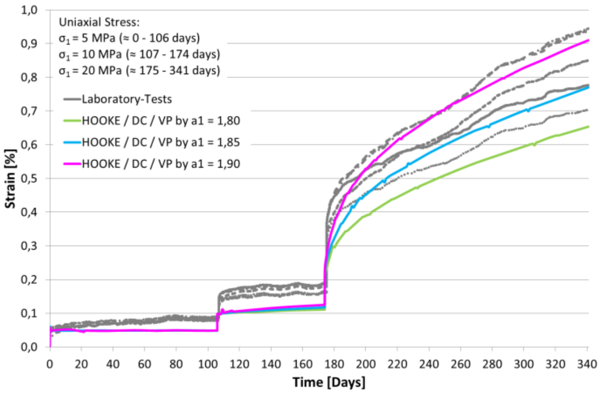

Fig. 4: Depiction of the deformation behaviour by considering EL, DC and VP model

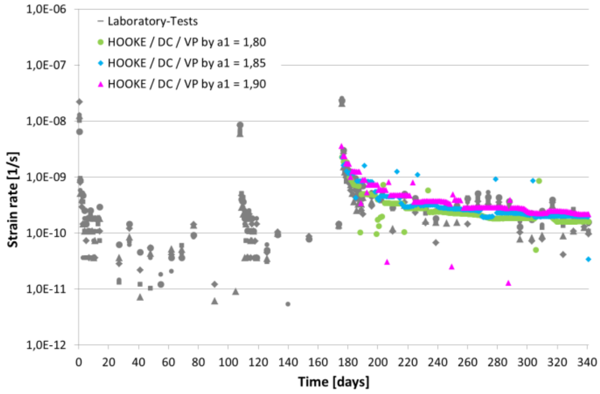

Fig. 2: Strains rates in third stress level

Additionally, strain rates reached a similar range as in the laboratory tests (Fig. 5). The evolution of porosity shows that porosity increases at the third stress level (not shown in the figures). So there is an interaction of elastic deformations, transient and stationary creep and dilatancy. This correlates to the assumptions from laboratory tests.

The final parameters used for the calculation of the uniaxial test in the third stress level are summarized in Tab. 2

LINEAR ELASTICITY	**E [MPa]**	**ν [-]**	**ϕ_0 [-]**		
	10.000	0.18	0.06		
DISLOCATION CREEP	**A_A [1/1*MPa^n]**	**Q_A [J/mol]**	**n [-|**		
	0.065e^{-6}	54.000	5		
VISCO-PLASTICITY	**m [-]**	**A [MPa^{-1}*s]**	**Q [J/mol]**	**a_6 [-]**	**W_d [-]**
	8	5*10^{-9}	54.000	0.02	3.5
	a_1 [-]	**a_2 [-]**	**a_3 [-]**	**a_4 [-]**	**a_5 [-]**
	1.8 – 1.9	1.8	2.5	0.7	0.02

Table 2: Classical constitutive laws used for physical modelling of salt concrete behaviour

3 CONCLUSIONS

The deformation behaviour of salt concrete was investigated by laboratory testing and numerical modelling. In the laboratory, two types of tests were carried out: Triaxial compression tests and uniaxial creep tests. The tests were simulated using CODE_BRIGHT and the calculation results were compared to the laboratory results.

The perceptions from the uniaxial tests in combination with the results from the triaxial tests showed that the material behaviour of salt concrete at an axial stress up to 10 MPa is different to the material behaviour at 20 MPa. Strains and strain rates clearly increase at higher stresses. The simulations showed that an adaptation to laboratory results was only possible if two different sets of parameters were used at the lower stress levels (phase 1) and the higher stress level (phase 2). The main problem of simulating the deformation behaviour of salt concrete is the description of the viscoplastic (transient creep) material behaviour. Elastic deformations and stationary creep can be adapted by the available material properties.

For a better description of transient material behaviour a constitutive model should be adapted or developed. The constitutive model used here allowed only a mathematical adaptation. Salt concrete consists of the cement matrix and the grains of salt concrete. This structure and its changes could not really be considered yet.

If the structure of salt concrete could be considered in detail, description of the deformation behaviour at different stress levels would become easier and clearer. Further investigations and developments in this direction are necessary. Further work is planned to be done within the framework of the DOPAS project.

4 ACKNOWLEDGEMENTS

The authors gratefully acknowledge the funding of the European Commission under FP7 framework programme, contract no. FP7-323273 the DOPAS project and the funding received by the Federal Ministry for Economics and Energy (BMWi), represented by the Project Management Agency Karlsruhe (PTKA-WTE), contract no. 02E11132.

REFERENCES

[i] Dopas (2012): DOPAS - full-scale demonstartion of plugs and seals, Annex 1: Description of work. Grant agreement no: 323273, Seventh framework programme, August 2012

[ii] CODE_BRIGHT, 2002. A 3D program for thermo-hydro-mechanical analysis in geological media. Users guide

[iii] Czaikowski, O., Hartwig, L., Hertes, U., Jantschik, K., Miehe, R., Müller, J., Schwarzianeck, P.: Full Scale Demonstration of Plugs and Seals (DOPAS) – Deliverable 5.11 – Status report on ELSA/LASA related laboratory tests and on process modelling activities, GRS-A-3760, Braunschweig, Februar 2015

MULTIPHASE FLOW MODELS OF CONCRETE CELLS OF THE RADIOACTIVE WASTE DISPOSAL FACILITY AT EL CABRIL (SPAIN)

M. Carme Chaparro* and Maarten W. Saaltink*

* GHS, Dept. Geotechnical Engineering and Geosciences, Technical University of Catalonia (UPC-BarcelonaTech), Campus Nord UPC, 08034 Barcelona, Spain, e-mail: m.carme.chaparro@upc.edu, maarten.saaltink@upc.edu

Key words: evaporation, condensation, multiphase flow, numerical models, concrete.

Abstract. *El Cabril is the low and intermediate level radioactive waste disposal facility for Spain. From the start of the filling (1992) until 2003, no water was collected from the drain situated at the centre of the cell. From 2003 onwards small amounts of water were collected from the drain, indicating flow of water within the cell. This occurred in summer and winter. A hypothesis had been proposed to explain this phenomenon based on multiphase flow and heat transport. We corroborate this hypothesis by means of 2D numerical models, using data measured by sensors in the cells and data from laboratory test. There is a good agreement between the data measured and the ones calculated by the models.*

1 INTRODUCTION

El Cabril is the low and intermediate level radioactive waste disposal facility for Spain, situated in Cordoba (South of Spain). The waste is stored in metal canisters, which are put in concrete containers, which in turn are placed in concrete cells. From the start of the filling (1992) until 2003, no water was collected from the drain situated at the center of the cell. From 2003 onwards small amounts of water were collected from the drain, indicating flow of water within the cell. This occurred during two distinctive periods each year: summer and winter.

This phenomenon could not be explained by infiltrating rainwater. The hypothesis proposed to explain this phenomenon consists of capillary flow through concrete and evaporation and condensation within the cell, produced by temperature gradients caused by seasonal temperature fluctuations outside. A key factor is a 2 cm gap between the wall of the cell and the containers with the radioactive waste.

Several studies have been conducted to explain this phenomenon [i,ii,iii, iv,v] using numerical models. However, these models are hypothetical because they do not use real data of temperature and relative humidity from the cells. Moreover, the hydraulic parameters used by the models are from literature. The objective of this work is to make numerical models of the cells using the data of temperature and relative humidity measured by sensors situated inside and outside the cells. Also we used thermo-hydraulic parameters of the concrete used to build the cells, which have been obtained from experimental test.

2 CONCEPTUAL MODEL

Figure 1 displays the conceptual model that explains the phenomena observed in the storage cells of El Cabril. Each concrete cell is 3 meters buried into the underlying rock and the rest of the cell is exposed to the atmosphere. The temperature inside the concrete cells (containers) is always 20ºC. Outside the temperature oscillates between around 40ºC in summer and around 5ºC in winter. These temperature oscillations outside the cell create a temperature difference between the two sides of an air gap existing between the concrete containers and the wall of the cell. There is a capillary flux through the wall of the cell. Moreover, the underlying rock and the wall of the cell are hydraulically connected. Evaporation is produced at the hot side (wall of the cell in summer and container in winter). The water vapour diffuses from the hotter side to the coldest side and condenses at the coldest side. Consequently, water runs off to the drain. This only occurs in summer and winter because only then the concrete reaches complete saturation.

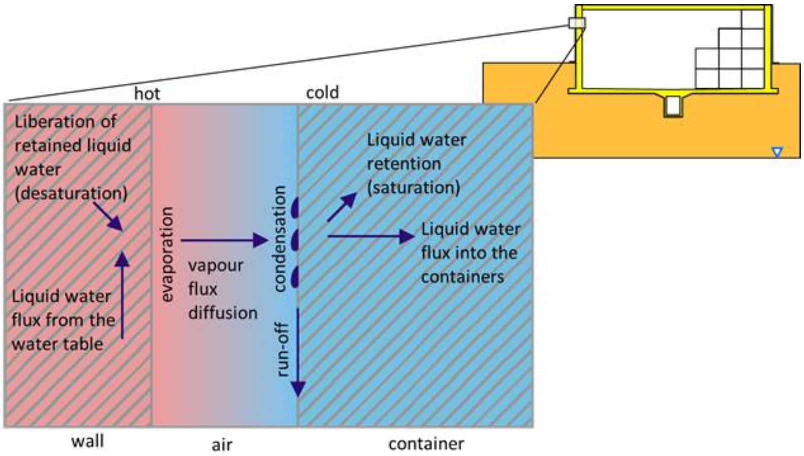

Figure 1: Conceptual model, scenario in summer [(i)].

In order to simulate these processes 2D numerical models have been built using CODE_BRIGHT [(vi)]. The geometry of the models takes into account the wall of the cell, the containers, the gap between them and the underlying rock. Balance equations of water, gas and energy are solved [(vii)]. A temperature of 19ºC in the entire cell has been considered as initial condition, and the initial liquid pressure decreases gradually from the water table (0.1 MPa) to the base of the cell (-0.9 MPa). A prescribed temperature boundary condition has been used, which also varies with time at the wall and the roof of the cell. We have used the daily average temperature measured by the sensors situated outside the cell. A leakage boundary condition has been applied to the gap of air between the wall and the container allowing water to leave the concrete wall only when liquid pressure exceeds atmospheric pressure. This represents the runoff water to the drain. Finally, at the bottom of the model the water table is simulated by fixing the liquid pressure to 0.1 MPa.

The Porosity and intrinsic permeability used in the numerical models were measured experimentally [viii, ix]. The retention curve, tortuosity, relative permeability and thermal conductivity have been obtained from Massana and Saaltink [ii].

3 RESULTS AND DISCUSSION

Figure 2 displays the results obtained from the numerical model. Sensors have been installed in the gap of air between wall and container in order to measure the temperature of the wall and the container. One of them is at the wall side and another one at the container side. Another sensor is located in the drain measuring the temperature inside the cell. Figure 2*a* shows the evolution of temperature measured by the sensors at 3.5 m from the base of the cell and the one calculated by the model. Two periods every year could be distinguished: summer where the temperature is around 30ºC and winter where the temperature is around 10ºC. The temperature at the wall has larger amplitude than that of the container, which means that the wall is hotter in summer and colder in winter thus causing a temperature difference. There is a good agreement between the model results and measured data by the sensors.

Figure 2*b* displays the saturation of the wall and the container calculated by the model. Similarly with temperature two periods of time every year can be distinguished. In summer, the wall has low saturation (around 0.6) and the container reaches complete saturation. The reverse occurs in winter. This verifies the hypothesis explaining the water can come out of the cell.

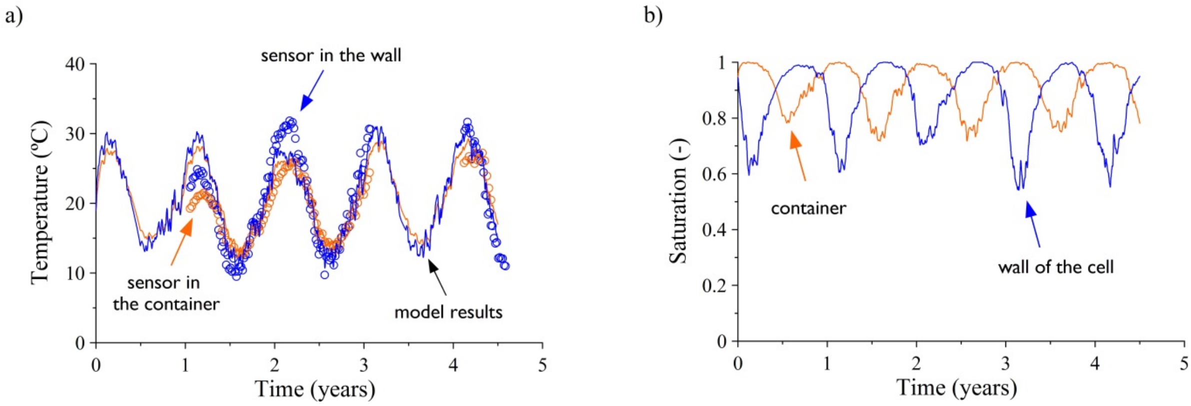

Figure 2: Results of the numerical model: a) temperature of the wall and the container; b) saturation of the wall and the container. Lines are the model results and points are the data measured by the sensors. Colour orange means container and blue means the wall of the cell.

4 CONCLUSIONS

The 2D numerical models can explain the fact that water can come out of the disposal cells due to evaporation and condensation processes inside the concrete and the thermohydraulic behaviour of the system.

- The temperature calculated by the model has a good agreement with the one measured by the sensors inside the cell
- The saturation calculated shows that in summer the wall of the cell is drier (around 0.6) and the wall of the concrete container is saturated (around 1). This corroborates the fact that the evaporation is produced at the hot side (the wall of the cell in summer and the container in winter) and condensation is produced at the cold side.

Acknowledgement. This work was funded by ENRESA (Spanish Nuclear Waste Management Company) and a Research Grant from the Technical University of Catalonia (UPC).

5 REFERENCES

[i] Saaltink, M.W., Sánchez-Vila, X., Carrera, J. (2005), Estudio cualitativo sobre la posibilidad que el agua recogida en la celda 16 proceda de un proceso de condensación. UPC Report, 28pp.

[ii] Massana, J., Saaltink, M.W. (2006), Modelo 2D de la celda 16. UPC Report, 27pp.

[iii] Zuloaga, P., Andrade, C., Saaltink, M.W. (2006) Long term water flow scenario in low-level waste disposal vaults, with particular regard to concrete structures in El Cabril, Cordoba, Spain. J.Phys IV, France, 136, 49-59.

[iv] Saaltink, M.W. (2006), Modelos bidimensionales de posibles medidas de remediación en las celdas de Cabril. UPC Report, 8pp.

[v] Gamazo, P., Saaltink, M.W., Carrera, J., Zuloaga, P. (2007) Modelación de procesos de evaporación y condensación en el interior de una celda de residuos. Estudios en la Zona no Saturada del Suelo, 8, 319-326.

[vi] Olivella, S., A. Gens, J. Carrera, E.E. Alonso (1996), Numerical formulation for a simulator (CODE_BRIGHT) for the coupled analysis of saline media, Eng. Comput.,13(7), 87-112.

[vii] Olivella, S., J. Carrera, A. Gens, E.E. Alonso (1994), Non-isotermal multiphase flow of brine and gas through saline media. Transport in porous Media. 15, 271-293.

[viii] Villar, M.V., Martín, P.L., Barcala, J.M. (2009) Caracterización del material de cobertera y el hormigón del C.A. El Cabril. CIEMAT Report CIEMAT/DMA/2G205/03/09, 55pp.

[ix] Villar, M.V. and Romero, F.J. (2014) Determination of water retention curves of concrete. 2nd International symposium on cement-based materials for nuclear waste (Nuwcem), Avignon, France, 2014, 1-9.

CRUSHED SALT DUMP MODELLING

Lin Jiang, Maria Teresa Yubero, Sebastià Olivella
Department of Geotechnical Engineering and Geosciences

In this research a conceptual framework on the genesis of tailings of salt mine is described. Based on recently published works, the main deformational mechanisms are also explained. The objective of this work is the study of the compaction process of waste salt materials due their self-weight since it is placed in the tailing pile. Dissolution and recrystallization phenomena are developed as a consequence of confining stresses and the water presence. It produces bonding between salt grains increasing the strength of the material and reductions of porosity. Intra-crystalline deformations also take place. This was investigated by means the modelling of a tailing deposit which includes the simulation of the construction and the long term response. In addition, a sensitivity analysis was performed.

An experimental program was carried out by Yubero (2008) on salt samples obtained from a tailing pile located at Súria (Spain) in order to establish the mechanical behaviour of the material. The experimental research was divided in two stages. First, the geotechnical profile could be determined from a comprehensive laboratory characterization. In a second stage, the behaviour of the salt aggregates was studied by means of oedometer tests on compacted samples. The material used was obtained from two different depths. Samples were saturated during two months using a salt solution under isothermal conditions (23ºC). Vertical stresses applied varied from 0,05 to 1,5MPa. Permeability measurements were obtained from oedometer tests (initial and final measurements) where a relationship between permeability and void ratio was established.

The experimental results were validated using the model constructed by CODE_BRIGHT for studying the mechanical behaviour of salt aggregates. The stress paths applied to each sample were modelled and numerical and experimental results were compared. Using this model, the strain velocity of the salt aggregates subjected to compaction under constant stress could be obtained. Moreover, the evolution of porosity and strength with time was also evaluated. The parameters are used to simulate the settlements of the tailing deposit.